Available online at www.sciencedirect.com
SCIENCE DIRECT®
Journal of Sound and Vibration 289 (2006) 529–550
JOURNAL OF SOUND AND VIBRATION
www.elsevier.com/locate/jsvi

Quantitative determination of material viscoelasticity using a piezoelectric cantilever bimorph beam

Jih-Lian Ha[a], Rong-Fong Fung[b,*], Sheng-Hsin Chang[b]

[a]*Department of Mechanical Engineering, Far East College, 49 Chung-Hua Road, Shin-Shi, Tainan, Taiwan 744, ROC*
[b]*Department of Mechanical and Automation Engineering, National Kaohsiung First University of Science and Technology, University Road, Yenchau, Kaohsiung 824, Taiwan, ROC*

Received 30 January 2004; received in revised form 26 August 2004; accepted 14 February 2005
Available online 4 June 2005

Abstract

The objective of this paper is to formulate the governing equation of a cantilever bimorph beam associated with a tip mass in contact with a viscoelastic material, which is modeled by a stiffness and a damper in parallel. From the eigenvalue problem, we can obtain the resonant frequencies as functions of the tip mass and material stiffness. The relation between the spectrum and material damping is established by the half-power bandwidth. It is found that the resonant frequencies increase as the material stiffness increases or the tip mass decreases, and the spectrum decreases by increasing the damping. From the analytic results, a cantilever could provide a technique to assess material viscoelasticity by simple measurements of the resonant frequency and the spectrum. Since the cantilever's behavior scales with its geometry, the device can be designed specifically for mechanical measurement of a microscopic system such as living cells and biomaterials.

1. Introduction

As the precision science develops allegro, the door is opened to the microcosm, i.e. the world of atomic. The scanning tunneling microscope, atomic force microscope (AFM) and their offshoots are the important keys [1] to open the door and they are referred to as the scanning probe

*Corresponding author. Tel.: +886 7 6011088; fax: +886 7 6011066.
E-mail address: rffung@ccms.nkfust.edu.tw (R.-F. Fung).

0022-460X/$ - see front matter © 2005 Elsevier Ltd. All rights reserved.
doi:10.1016/j.jsv.2005.02.024

microscope. The atomic force between the microcantilever tip and sample is employed during the process of measurement. The AFM, with its ability to image surface on the nanometer scale, offers the potential to measure directly the viscoelasticity of living cells and biomaterials. Some important observations of the AFM were made from the governing equations and boundary conditions [2].

In recent years, mechanical devices using piezoelectric effects have drawn much attention both scientifically and technologically, because a piezoelectric actuator is able to control a micrometer displacement accurately and quickly. The microcantilevers have made it possible to build new sensors, which are simple, compact and easy to operate, for measuring magnetic susceptibilities of nanogram materials [3], the swelling or volume expansion experienced by an active sensing material [4], the solution pH [5], material damping [6] and Young's modulus [7].

This paper studies the dynamic behavior of a stepped piezoelectric cantilever beam, which is composed of two piezoelectric layers and one sandwiched nickel layer. The dynamic formulation based on the general concept of constitutive laws of piezoelectric material [8] is derived by Hamilton's principle. In order to obtain the relations of resonant frequencies with respect to the tip mass and material stiffness, the eigenvalue problem is solved. Some observations from the governing equations, transition conditions, continuous conditions and boundary conditions are discussed. Finally, the numerical method using the finite element method is provided to illustrate the dynamic responses and their spectrum for the piezoelectric cantilever bimorph beams. Consequentially, the material stiffness can be obtained from the eigenvalue problem and the material damper can be calculated from the half-power bandwidth of the frequency spectrum.

2. Dynamic model development

2.1. Physical model

The system model shown in Fig. 1 is a parallel connection of the piezoelectric bimorph beam. The two piezoelectric layers are used as the actuator. The directions of big arrows represent the polarization directions of the piezoelectric layers. For the microcantilever beam, the slenderness ratio is very small, and Euler-beam theory is suitable to describe its behavior. First of all, Hamilton's principle [9,10] will be employed to derive the equations off motion for the piezoelectric bimorph system.

2.2. Equations of motion

In order to formulate the equations of motion, the cantilever beam is divided into two regions: the triple-layer beam $0<x<\ell_p$ and the nickel beam $\ell_p<x<\ell_b$. The subscripts p and b are denoted for the piezoceramic bimorph and the nickel beam, respectively. The cantilever is a flexible beam with length ℓ_b, width w_b and thickness t_b. The tip mass is a pyramid rigid segment with height h, thickness 2ℓ and width w. The unknown material stiffness and damping coefficient are assumed as k and c, respectively. The tip mass could be in another sense of describing the equivalent mass of material stiffness, which is assumed massless in the dynamic modeling. The distance between the

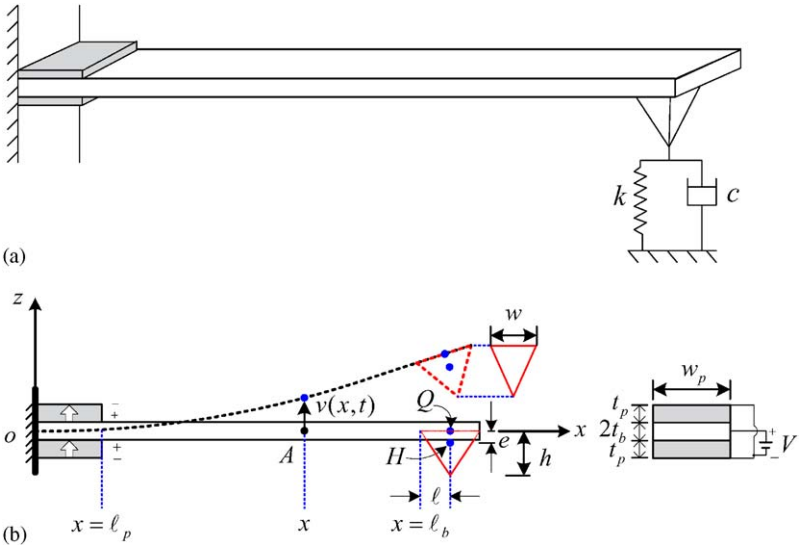

Fig. 1. Schematic diagrams: (a) the piezoelectric cantilever bimorph beam; (b) the deformed configuration.

point Q and the geometric center H is e. The oxz coordinate system is employed to describe the planar motion. The electric field and applied voltage direct along the z-axis.

2.3. Kinetic and strain energies

The neutral-axis displacements of an arbitrary point A of the piezoelectric cantilever beam are

$$u_1(x,z,t) = -zv_x(x,t), \quad u_3(x,z,t) = v(x,t), \tag{1}$$

where $v(x,t)$ represents the transverse displacement. The subscript x represents the spatial derivative. The position vector after deformation is

$$\mathbf{R}_A(x,z,t) = [x - zv_x(x,t)]\mathbf{i} + [z + v(x,t)]\mathbf{k}. \tag{2}$$

The deformed position vector of the mass center point H is

$$\mathbf{R}_H(x,z,t) = (\ell_b + l)\mathbf{i} + [z + v(\ell_b,t) + \ell v_x(\ell_b,t) - e]\mathbf{k}. \tag{3}$$

Therefore, the total kinetic energy of the cantilever system including the tip mass can be expressed as

$$T = \frac{1}{2}\int_{V_p} \rho_p \frac{\mathrm{d}}{\mathrm{d}t}\mathbf{R}_A \cdot \frac{\mathrm{d}}{\mathrm{d}t}\mathbf{R}_A \,\mathrm{d}V_p\Big|_{\text{upper}} + \frac{1}{2}\int_{V_p} \rho_p \frac{\mathrm{d}}{\mathrm{d}t}\mathbf{R}_A \cdot \frac{\mathrm{d}}{\mathrm{d}t}\mathbf{R}_A \,\mathrm{d}V_p\Big|_{\text{lower}}$$
$$+ \frac{1}{2}\int_{V_b} \rho_b \frac{\mathrm{d}}{\mathrm{d}t}\mathbf{R}_A \cdot \frac{\mathrm{d}}{\mathrm{d}t}\mathbf{R}_A \,\mathrm{d}V_b + \frac{1}{2}m\frac{\mathrm{d}}{\mathrm{d}t}\mathbf{R}_H \cdot \frac{\mathrm{d}}{\mathrm{d}t}\mathbf{R}_H$$

$$= \frac{1}{2}\int_0^{\ell_p} \rho_p A_p v_t^2(x,t)\,\mathrm{d}x\bigg|_{\text{upper}} + \frac{1}{2}\int_0^{\ell_p} \rho_p A_p v_t^2(x,t)\,\mathrm{d}x\bigg|_{\text{lower}} + \int_0^{\ell_b} \rho_b A_b v_t^2(x,t)\,\mathrm{d}x$$
$$+ \frac{1}{2} m[v_t(\ell_b,t) + \ell v_{xt}(\ell_b,t)]^2$$
$$= \int_0^{\ell_p} \rho A v_t^2(x,t)\,\mathrm{d}x + \int_{\ell_p}^{\ell_b} \rho_b A_b v_t^2(x,t)\,\mathrm{d}x + \frac{1}{2} m[v_t(\ell_b,t) + \ell v_{xt}(\ell_b,t)]^2, \tag{4}$$

where $\rho A = \rho_p A_p + \rho_b A_b$, $\rho_p A_p = \rho_p A_p|_{\text{upper}} + \rho_p A_p|_{\text{lower}}$, ρ is the mass density, A is the total cross-sectional area of the triple-layer beam, $A_p = w_p t_p$ and $A_b = w_b t_b$. The subscript t represents the time derivative. It is noted that the piezoelectric term with subscript p exists only for the region $0 < x < \ell_p$ and the electric field has no influence on the region $\ell_p < x < \ell_b$. In Eq. (4), the rotary inertia is neglected for the Euler-beam assumption.

The Lagrangian strains of the piezoelectric cantilever beam are

$$\varepsilon_{b11} = \varepsilon_{p11} = -z v_{xx}, \quad \varepsilon_{b12} = \varepsilon_{p12} = 0, \quad \varepsilon_{b13} = \varepsilon_{b31} = \varepsilon_{p13} = \varepsilon_{p31} = 0. \tag{5}$$

If an electrical field E_3 is applied across the thickness direction of the piezoelectric bimorph with parallel polarity, the constitutive equations for these two piezoelectric layers will be

$$\text{The upper layer:} \quad \begin{bmatrix} \sigma_{p11} \\ E_{3\text{upper}} \end{bmatrix} = \begin{bmatrix} E_p & -h_{31} \\ -h_{31} & \beta_{33} \end{bmatrix} \begin{bmatrix} \varepsilon_{p11} \\ D_{33} \end{bmatrix}, \tag{6}$$

$$\text{The lower layer:} \quad \begin{bmatrix} \sigma_{p11} \\ E_{3\text{lower}} \end{bmatrix} = \begin{bmatrix} E_p & -h_{31} \\ -h_{31} & \beta_{33} \end{bmatrix} \begin{bmatrix} \varepsilon_{p11} \\ -D_{33} \end{bmatrix}, \tag{7}$$

where D_{33} and E_p are the electrical displacement and Young's modulus of the piezoelectric layers along the z-direction, respectively; ε_{p11} and σ_{p11} are the mechanical strain and stress in the x-direction, respectively. $E_{3\text{upper}}$ and $E_{3\text{lower}}$ are the electric fields applied to the upper and lower piezoelectric layers, respectively. β_{33} is the dielectric constant and h_{31} is the piezoelectric constant.

The potential energy of the cantilever bimorph beam including the material stiffness attached at the tip mass is

$$U = U_p + U_b + U_k$$
$$= \frac{1}{2}\int_{V_p} (\sigma_{p11}\varepsilon_{p11} + D_{33}E_{3\text{upper}})\,\mathrm{d}V_p\bigg|_{\text{upper}} + \frac{1}{2}\int_{V_p} (\sigma_{p11}\varepsilon_{p11} + D_{33}E_{3\text{lower}})\,\mathrm{d}V_p\bigg|_{\text{lower}}$$
$$+ \frac{1}{2}\int_{V_b} \sigma_{b11}\varepsilon_{b11}\,\mathrm{d}V_b + \frac{1}{2} k[v(\ell_b,t) + \ell v_x(\ell_b,t)]^2$$
$$= \int_0^{\ell_p} EI v_{xx}^2\,\mathrm{d}x + \int_0^{\ell_p} D_{33}h_{31}A_p v_{xx}(t_p + 2t_b)\,\mathrm{d}x + \int_0^{\ell_p} \beta_{33}A_p D_{33}^2\,\mathrm{d}x$$
$$+ \int_{\ell_p}^{\ell_b} [E_b I_b v_{xx}^2(x,t)]\,\mathrm{d}x + \frac{1}{2} k[v(\ell_b,t) + \ell v_x(\ell_b,t)]^2, \tag{8}$$

where $EA = E_pA_p + E_bA_b$, $EI = E_pI_p + E_bI_b$, $I_p = \int_{A_p} z^2\,\mathrm{d}A_p$, $I_b = \int_{A_b} z^2\,\mathrm{d}A_b$, and E_b is the Young's modulus of the cantilever nickel beam.

The virtual work done by the electrical voltage V_{cc}, the material damping c and the initially normal force f acting on the tip is

$$\delta W = 2\int_0^{\ell_p} V_{cc}w_p\delta D_{33}(x,t)\,\mathrm{d}x + \{f - c[v_t(\ell_b,t) + \ell v_{xt}(\ell_b,t)]\}\delta[v(\ell_b,t) + \ell v_x(\ell_b,t)]. \tag{9}$$

2.4. Hamilton's principle

By using Hamilton's principle [9,10]

$$\int_{t_1}^{t_2} [\delta(T-U) + \delta W]\,\mathrm{d}t = 0, \tag{10}$$

we obtain the governing equations for each region of the piezoelectric cantilever bimorph beam:

$$v_i : \rho_i A_i v_{itt} + E_i I_i v_{ixxxx} = 0,$$
$$i = 1 \text{ for } 0<x<\ell_p \text{ and } i = 2 \text{ for } \ell_p<x<\ell_b, \tag{11a, b}$$

$$D_{33} : -(t_p + 2t_b)A_p h_{31} v_{1xx} + 2V_{cc}w_p - 2A_p\beta_{33}D_{33} = 0, \quad 0<x<\ell_p, \tag{11c}$$

where $\rho_1A_1 = \rho_pA_p + \rho_bA_b$, $\rho_2A_2 = \rho_bA_b$, $E_1I_1 = E_pI_p + E_bI_b$ and $E_2I_2 = E_bI_b$.

The boundary conditions at $x = 0$ and ℓ_b are

$$x = 0:$$
$$v_1(0,t) = 0, \quad v_{1x}(0,t) = 0,$$
$$x = \ell_b:$$
$$m[v_{2tt}(\ell_b,t) + \ell v_{2xtt}(\ell_b,t)] + c[v_t(\ell_b,t) + \ell v_{xt}(\ell_b,t)] + k[v_2(\ell_b,t) + \ell v_{2x}(\ell_b,t)] - E_bI_b v_{2xxx}(\ell_b,t) = f, \tag{12a, b}$$

$$m\ell[v_{2tt}(\ell_b,t) + \ell v_{2xtt}(\ell_b,t)] + c\ell[v_t(\ell_b,t) + \ell v_{xt}(\ell_b,t)] + k\ell[v_2(\ell_b,t) + \ell v_{2x}(\ell_b,t)] + E_bI_b v_{2xx}(\ell_b,t) = f\ell. \tag{12c, d}$$

From Eq. (11c), we have the electric displacement

$$D_{33} = \frac{2V_{cc}w_p - (t_p + 2t_b)A_p h_{31} v_{1xx}}{2A_p\beta_{33}}, \tag{13}$$

which is caused by the external voltage V_{cc} and the curvature v_{1xx}. By using Eq. (13) for the two adjacent regions, $0<x<\ell_p$ and $\ell_p<x<\ell_b$, from Eq. (10) we have the transition conditions at $x = \ell_p$:

$$E_2I_2v_{2xxx}(\ell_p^+,t) = E_1I_1v_{1xxx}(\ell_p^-,t), \tag{14a}$$

$$E_2I_2v_{2xx}(\ell_p^+,t) - \left[E_1I_1 - \frac{h_{31}^2A_p(t_p+2t_b)^2}{4\beta_{33}}\right]v_{1xx}(\ell_p^-,t) = \frac{1}{2}m_v, \tag{14b}$$

where $m_v = (t_p + 2t_b)h_{31}V_{cc}w_p/\beta_{33}$ is the moment induced by the external voltage V_{cc}. In the manipulation of Eq. (14), we have used the following continuous conditions:

$$v_1(\ell_p^-, t) = v_2(\ell_p^+, t), \tag{15}$$

$$v_{1x}(\ell_p^-, t) = v_{2x}(\ell_p^+, t). \tag{16}$$

2.5. Discussion

From the governing equations (11a,b), boundary conditions (12a–d) and transition conditions (14a, b) of the system, the following observations are made:

(1) The governing equations (11a,b) for the transverse displacements are homogeneous. Transition condition (14a) describes the continuity of the shear force. The applied voltage V_{cc} becomes an external moment, and appears in the transition condition (14b). The moment causes the jump of bending curvature at the point $x = \ell_p$.
(2) When an electric filed is applied to the two parallel piezoelectric layers of the cantilever beam, the upper layer expands but the lower layer contracts along the length direction. This will produce a pure bending moment and is mathematically seen from Eq. (14b).
(3) The piezoelectric bimorph is suitable to actuate the cantilever beam because that only the bending moment m_v is produced by the applied voltage. Based on the Euler beam's assumption, the beam is bent and the length of the neutral axis remains unchanged when an external voltage is applied.
(4) Under the external voltage, the piezoelectric cantilever bimorph beam produces a pure bending deformation. Such a model is feasible to be designed as a measuring device, which is affixed as tip mass at the free end and is shown in Fig. 1.

2.6. Eigenvalue problem

For the convenience in search of the behavior of the system parameter, we define the following dimensionless variables and parameters:

$$V_1 = \frac{v_1}{\ell_b}, \quad V_2 = \frac{v_2}{\ell_b}, \quad \xi = \frac{x}{\ell_b}, \quad \mu = \frac{\ell_p}{\ell_b}, \quad \tau = \omega_T t, \quad L = \frac{\ell}{\ell_b}, \quad M_v = \frac{m_v}{E_b I_b},$$

$$M = \frac{m}{\rho_b A_b \ell_b}, \quad K = \frac{k\ell_b^3}{E_b I_b}, \quad \bar{C} = \frac{c\ell_b}{4\pi\sqrt{\rho_b A_b E_b I_b}}, \quad F = \frac{f}{\rho_b A_b \ell_b^2 \omega_T^2}, \quad \omega_T^2 = \frac{\pi^4 E_b I_b}{\rho_b A_b \ell_b^4}.$$

Substituting them into Eqs. (11a,b) and (12a–d), we have the dimensionless governing equation

$$a_i \frac{\mathrm{d}^4 V_i(\xi,\tau)}{\mathrm{d}\xi^4} + b_i \pi^4 \frac{\mathrm{d}^2 V_i(\xi,\tau)}{\mathrm{d}\tau^2} = 0, \quad i = 1 \text{ for } 0 < \xi < \mu \quad \text{and} \quad i = 2 \text{ for } \mu < \xi < 1, \tag{17}$$

where

$$a_1 = \frac{E_p I_p + E_b I_b}{E_b I_b}, \quad b_1 = \frac{\rho_p A_p + \rho_b A_b}{\rho_b A_b} \quad \text{and} \quad a_2 = b_2 = 1.$$

The continuous conditions become

$$V_1(\mu^-,\tau) = V_2(\mu^+,\tau), \tag{18}$$

$$V_{1\xi}(\mu^-,\tau) = V_{2\xi}(\mu^+,\tau). \tag{19}$$

The transition conditions become

$$a_1 V_{1\xi\xi\xi}(\mu^-,\tau) - V_{2\xi\xi\xi}(\mu^+,\tau) = 0, \tag{20}$$

$$-\gamma V_{1\xi\xi}(\mu^-,\tau) + V_{2\xi\xi}(\mu^+,\tau) = \tfrac{1}{2} M_v, \tag{21}$$

where

$$\gamma = a_1 - \frac{h_{31}^2 A_p (t_p + 2t_b)^2}{4\beta_{33} E_b I_b}.$$

The boundary conditions become

$$V_1(0,\tau) = 0, \quad V_{1\xi}(0,\tau) = 0, \tag{22, 23}$$

$$M[V_{2\tau\tau}(1,\tau) + LV_{2\xi\tau\tau}(1,\tau)] + \bar{C}[V_{2\tau}(1,\tau) + LV_{2\xi\tau}(1,\tau)] + \frac{K}{\pi^4}[V_2(1,\tau) + LV_{2\xi}(1,\tau)] - \frac{1}{\pi^4} V_{2\xi\xi\xi}(1,\tau) = F, \tag{24}$$

$$ML[V_{2\tau\tau}(1,\tau) + LV_{2\xi\tau\tau}(1,\tau)] + \bar{C}L[V_{2\tau}(1,\tau) + LV_{2\xi\tau}(1,\tau)] + \frac{1}{\pi^4} KL[V_2(1,\tau) + LV_{2\xi}(1,\tau)] + \frac{1}{\pi^4} V_{2\xi\xi}(1,\tau) = FL. \tag{25}$$

In order to obtain the eigenvalue problem, the damping $\bar{C}$, the initially normal force F and the bending moment M_v are neglected in this section. For the discrete systems, we explore the circumstance under which the motion of the beam is synchronous [10]. In mathematical terminology, such a solution $V_i(\xi,\tau)$ of the boundary-value problem (17) and Eqs. (22–25), is said to be separable in the spatial variable ξ and the time τ, and can be expressed in the form

$$V_i(\xi,\tau) = \Phi_i(\xi) T(\tau), \quad i = 1, 2, \tag{26}$$

where $\Phi_i(\xi)$ represents the beam shape, and is a function of ξ alone, and $T(\tau)$ indicates how the amplitude varies with time τ.

By using the method of separation of variables, we have the following boundary value problem:

$$\frac{\mathrm{d}^2}{\mathrm{d}\xi^2}\left[\frac{\mathrm{d}^2\Phi_i(\xi)}{\mathrm{d}\xi^2}\right] - \beta_i^4 \Phi_i(\xi) = 0, \quad 0 < \xi < 1, \tag{27}$$

where $\beta_i^4 = (\pi^4 b_i/a_i)\omega^2$, $i = 1, 2$, and the solution must satisfy the boundary conditions (22–25). It is noted that one natural frequency ω and two eigenvalues β_1 and β_2 exist in this problem of the cantilever beam being divided into two regions.

Inserting Eq. (26) into Eqs. (18–25) and dividing by $T(\tau)$, the continuous conditions (18, 19), transition conditions (20, 21) and boundary conditions (22–25) reduce to

$$\Phi_1(\mu^-) = \Phi_2(\mu^+), \tag{28}$$

$$\Phi_{1\xi}(\mu^-) = \Phi_{2\xi}(\mu^+), \tag{29}$$

$$a_1\Phi_{1\xi\xi\xi}(\mu^-) = \Phi_{2\xi\xi\xi}(\mu^+), \tag{30}$$

$$\Phi_{2\xi\xi}(\mu^+) - \gamma\Phi_{1\xi\xi}(\mu^-) = 0, \tag{31}$$

$$\Phi_1(0) = 0, \quad \frac{d\Phi_1(0)}{d\xi} = 0, \tag{32, 33}$$

$$\frac{d}{d\xi}\left[\frac{d^2\Phi_2(1)}{d\xi^2}\right] - K\left[\Phi_2(1) + L\left(\frac{d\Phi_2(1)}{d\xi}\right)\right] + \beta_2^4 M\left[\Phi_2(1) + L\left(\frac{d\Phi_2(1)}{d\xi}\right)\right] = 0, \tag{34}$$

$$\frac{d^2\Phi_2(1)}{d\xi^2} + KL\left[\Phi_2(1) + L\left(\frac{d\Phi_2(1)}{d\xi}\right)\right] - \beta_2^4 ML\left[\Phi_2(1) + L\left(\frac{d\Phi_2(1)}{d\xi}\right)\right] = 0. \tag{35}$$

The problem of determining the constant ω^2 such that Eq. (27) admits nontrivial solutions $\Phi_i(\xi)$ satisfying conditions (28)–(35) is known as the *differential eigenvalue problem* [10].

The solution of Eq. (27) can be verified as

$$\Phi_i(\xi) = A_i \ \sin\beta_i\xi + B_i \ \cos\beta_i\xi + C_i \ \sinh\beta_i\xi + D_i \ \cosh\beta_i\xi, \tag{36}$$

where A_i, B_i, C_i and D_i, $i = 1, 2$ are constants to be determined by using conditions (28–35). The detailed results can be seen in Appendix A.

By using conditions (28–35), we can obtain the characteristic equation for β_i:

$$\begin{bmatrix} \alpha_{11} & \alpha_{12} & \alpha_{13} & \alpha_{14} \\ \alpha_{21} & \alpha_{22} & \alpha_{23} & \alpha_{24} \\ \alpha_{31} & \alpha_{32} & \alpha_{33} & \alpha_{34} \\ \alpha_{41} & \alpha_{42} & \alpha_{43} & \alpha_{44} \end{bmatrix} \begin{bmatrix} A_2 \\ B_2 \\ C_2 \\ D_2 \end{bmatrix} = 0, \tag{37}$$

where α_{ij}, $i,j = 1, 2, \ldots, 4$ are detailed in Ref. [11]. The characteristic Eq. (37) will be employed to determine the resonant frequencies with respect to the different material stiffnesses and various values of tip masses.

By using the determinant $|\alpha_{ij}| = 0$, $i,j = 1, 2, \ldots, 4$ of the characteristic Eq. (37), rather than using the relationship between the exciting frequency and the tip displacement [12], we could obtain the relationship between the eigenvalue and the material stiffness. The detailed procedure of calculating the material stiffness can be seen in Section 5.2.

2.7. Comparison

As the tip mass is neglected in Ref. [12], the numerical result is larger than the experimental data, because the resonant frequency decreases by increasing the tip mass. This paper proposes the complete analysis of the relationship between the resonant frequencies with the material stiffnesses and the tip masses.

If the two piezoelectric layers, the damper and tip mass are neglected, the characteristic Eq. (37) is the same as that in Ref. [13] by neglecting the length extending from the spring to the free end.

If the two piezoelectric layers, the damper and material stiffness are neglected, the characteristic Eq. (37) is the same as that of Ref. [14].

2.8. A simple case and sensitivity analysis

In addition, if the two piezoelectric layers are neglected, we can obtain the closed-form characteristic equation for β:

$$\frac{1+\cos\beta\cosh\beta}{\sin\beta\cosh\beta-\sinh\beta\cos\beta+2\beta L\sin\beta\sinh\beta+(\beta L)^2(\cos\beta\sinh\beta+\cosh\beta\sin\beta)} = -\frac{K-\beta^4 M}{\beta^3}. \tag{38}$$

If $\ell_b \gg \ell$, we have $L \approx 0$, and the above characteristic equation becomes

$$\frac{1+\cos\beta\cosh\beta}{\sin\beta\cosh\beta-\sinh\beta\cos\beta} = -\frac{K-\beta^4 M}{\beta^3}. \tag{39}$$

The above characteristic Eq. (39) will be employed to determine numerically the first and second resonant frequencies with respect to the different material stiffnesses and various values of tip masses.

Differentiating Eq. (39) with respect to β, and inversing the results, we obtain the derivative of β with respect to K by treating $\mathrm{d}M/\mathrm{d}\beta = 0$, and the derivative of β with respect to M by treating $\mathrm{d}K/\mathrm{d}\beta = 0$. Thus, the first-order sensitivity analysis can be written as follows:

$$\begin{aligned}\frac{\mathrm{d}\beta}{\mathrm{d}K} = {} & (\sin\beta\cosh\beta-\sinh\beta\cos\beta)^2/[4\beta^3 M(\sin\beta\cosh\beta-\sinh\beta\cos\beta)^2 \\ & -3\beta^2(1+\cos\beta\cosh\beta)(\sin\beta\cosh\beta-\sinh\beta\cos\beta) \\ & +\beta^3(\sin^2\beta\cosh^2\beta+\sinh^2\beta\cos^2\beta+2\sin\beta\sinh\beta)],\end{aligned} \tag{40}$$

$$\begin{aligned}\frac{\mathrm{d}\beta}{\mathrm{d}M} = {} & -\beta^5(\sin\beta\cosh\beta-\sinh\beta\cos\beta)^2/[4K(\sin\beta\cosh\beta-\sinh\beta\cos\beta) \\ & +\beta^3(1+\cos\beta\cosh\beta)(\sin\beta\cosh\beta-\sinh\beta\cos\beta) \\ & +\beta^4(\sin^2\beta\cosh^2\beta+\sinh^2\beta\cos^2\beta+2\sin\beta\sinh\beta)].\end{aligned} \tag{41}$$

3. Damping determination from half-power bandwidth

One common method [15,16] of determining damping ratio is to measure the spectrum bandwidth between points on the response curve, for which the response is some fraction of the resonance spectrum of the system. In this paper, the half-power bandwidth of the frequency spectrum is adopted to determine the material damping ratio.

Consider the viscous damping system shown in Fig. 1(a). The magnification factor (MF) can be obtained in the following relation:

$$\mathrm{MF} = \{[1-(\omega_c/\omega_r)^2]^2 + 4\zeta^2\}^{-1/2}, \tag{42}$$

where ω_r is the frequency of maximum amplitude and ω_c is the circular frequency of vibration. It is easily seen that the MF is a function of only two parameters: the frequency ratio (ω_c/ω_r) and the damping ratio (ζ).

The resonant magnification factor (RMF) is defined as the value of the MF at resonance. Thus, the half-power magnification factor (HPMF) with the power being one-half of that at resonance is related to the damping ratio as follows [15]:

$$\text{HPMF} = \text{RMF}/\sqrt{2} = \left(2\sqrt{2}\zeta\right)^{-1}. \tag{43}$$

Combining Eqs. (42) and (43), the two half-power frequencies ($\omega_r^{(1)}$ and $\omega_r^{(2)}$) corresponding to half-power could be obtained as

$$\omega_r^{(1),(2)} = \omega_r(1 \pm 2\zeta)^{1/2}. \tag{44}$$

For small damping ratio ($\zeta \ll 1/2$), the above equation could be simple as

$$\omega_r^{(1),(2)} \approx \omega_r(1 \pm \zeta). \tag{45}$$

Thus, we get the following relation between the dimensionless bandwidth and the damping ratio:

$$\frac{\omega_r^{(2)} - \omega_r^{(1)}}{\omega_r} \approx 2\zeta. \tag{46}$$

4. Finite element method

By using the standard finite element technique [17] and assembling the equation of motion, we obtain a set of ordinary differential equations for the piezoelectric cantilever bimorph beam:

$$\mathbf{M}\ddot{\mathbf{Q}} + \mathbf{C}\dot{\mathbf{Q}} + \mathbf{K}\mathbf{Q} = \mathbf{F}, \tag{47}$$

where $\mathbf{Q}$ is the global displacement vector, $\mathbf{M}$, $\mathbf{C}$ and $\mathbf{K}$ are the global mass, damping and stiffness matrices, respectively, $\mathbf{F}$ is a force vector which includes the external voltage $V_{cc}(t)$ and the initially normal force f, and

$$\mathbf{Q} = [q_1 \cdots q_n \cdots q_{2n}]^{\mathrm{T}} 1 \times 2n, \tag{48}$$

$$\mathbf{M} = \sum_{j=1}^{n} 2\rho A \int_0^{\ell_p} \mathbf{N}_j^{\mathrm{T}}\mathbf{N}_j \,\mathrm{d}x + 2\rho_b A_b \int_{\ell_p}^{\ell_b} \mathbf{N}_j^{\mathrm{T}}\mathbf{N}_j \,\mathrm{d}x + m\{\mathbf{N}(\ell_b)^{\mathrm{T}}\mathbf{N}(\ell_b) + \ell[\mathbf{N}(\ell_b)^{\mathrm{T}}\mathbf{B}(\ell_b) + \mathbf{B}(\ell_b)^{\mathrm{T}}\mathbf{N}(\ell_b)] + \ell^2\mathbf{B}(\ell_b)^{\mathrm{T}}\mathbf{B}(\ell_b)\}, \tag{49}$$

$$\mathbf{C} = c\{\mathbf{N}(\ell_b)^{\mathrm{T}}\mathbf{N}(\ell_b) + \ell[\mathbf{N}(\ell_b)^{\mathrm{T}}\mathbf{B}(\ell_b) + \mathbf{B}(\ell_b)^{\mathrm{T}}\mathbf{N}(\ell_b)] + \ell^2\mathbf{B}(\ell_b)^{\mathrm{T}}\mathbf{B}(\ell_b)\}, \tag{50}$$

$$\mathbf{K} = \sum_{j=1}^{n} 2EI \int_0^{\ell_p} \mathbf{D}_j^{\mathrm{T}}\mathbf{D}_j \,\mathrm{d}x + 2E_bI_b \int_{\ell_p}^{\ell_b} \mathbf{D}_j^{\mathrm{T}}\mathbf{D}_j \,\mathrm{d}x - \frac{h_{31}^2(2t_b + t_p)^2 A_p}{\beta_{33}} \int_0^{\ell_p} \mathbf{D}_j^{\mathrm{T}}\mathbf{D}_j \,\mathrm{d}x + k[\mathbf{N}(\ell_b)^{\mathrm{T}}\mathbf{N}(\ell_b) + \ell(\mathbf{N}(\ell_b)^{\mathrm{T}}\mathbf{B}(\ell_b) + \mathbf{B}(\ell_b)^{\mathrm{T}}\mathbf{N}(\ell_b)) + \ell^2\mathbf{B}(\ell_b)^{\mathrm{T}}\mathbf{B}(\ell_b)], \tag{51}$$

$$\mathbf{F} = \sum_{j=1}^{n} -\frac{h_{31}V_{cc}b(2h + h_p)}{\beta_{33}} \int_0^{\ell_p} \mathbf{D}_j^{\mathrm{T}} \,\mathrm{d}x + f[\mathbf{N}(\ell_b)^{\mathrm{T}} + \ell\mathbf{B}(\ell_b)^{\mathrm{T}}], \tag{52}$$

where $\mathbf{N}$ is the shape function, $\mathbf{B} = (\mathrm{d}/\mathrm{d}x)\mathbf{N}$ and $\mathbf{D} = (\mathrm{d}^2/\mathrm{d}x^2)\mathbf{N}$. The details can be seen in Ref. [11].

It is assumed that the damping of the cantilever beam is negligible when compared with the material damping. Thus, only the material damping constructs the damping matrix $\mathbf{C}$, which is to be measured. In the present study, the global damping matrix $\mathbf{C}$ can be written as

$$\mathbf{C} = \begin{bmatrix} \mathbf{0} & \mathbf{0} \\ \mathbf{0} & \mathbf{C}_d \end{bmatrix} = \bar{\alpha} \begin{bmatrix} \mathbf{0} & \mathbf{0} \\ \mathbf{0} & \mathbf{M}_d \end{bmatrix} + \bar{\beta} \begin{bmatrix} \mathbf{0} & \mathbf{0} \\ \mathbf{0} & \mathbf{K}_d \end{bmatrix}, \tag{53}$$

where it is assumed that the material damping is described by the proportional damping [18]:

$$\mathbf{C}_d = \bar{\alpha}\mathbf{M}_d + \bar{\beta}\mathbf{K}_d, \tag{54}$$

in which $\mathbf{M}_d$ and $\mathbf{K}_d$ are the 2×2 sub-matrices of $\mathbf{M}$ and $\mathbf{K}$, respectively, and $\bar{\alpha}$ and $\bar{\beta}$ are two constants to be determined from frequency spectrum.

Premultiplying Eq. (54) by $\mathbf{U}_d^{\mathrm{T}}$ and postmultiplying by $\mathbf{U}_d$, we have

$$\mathbf{U}_d^{\mathrm{T}}\mathbf{C}_d\mathbf{U}_d = \bar{\alpha}\mathbf{U}_d^{\mathrm{T}}\mathbf{M}_d\mathbf{U}_d + \bar{\beta}\mathbf{U}_d^{\mathrm{T}}\mathbf{K}_d\mathbf{U}_d = \bar{\alpha}\mathbf{I} + \bar{\beta}\mathbf{\Omega}, \tag{55}$$

where the orthonormal conditions for the sub-matrices $\mathbf{M}_d$ and $\mathbf{K}_d$ are used. The relationship [10] among $\bar{\alpha}, \bar{\beta}, \zeta_r$ and ω_r can be obtained as

$$\bar{\alpha} + \bar{\beta}\omega_r^2 = 2\zeta_r\omega_r, \quad r = 1, 2, \ldots . \tag{56}$$

By inspecting the frequency spectrum, we could obtain ω_r, $\omega_r^{(1)}$ and $\omega_r^{(2)}$. Then, the damping ratio ζ_r is calculated for each mode by using Eq. (46). The two constants $\bar{\alpha}$ and $\bar{\beta}$ in Eq. (56) can be obtained by using the ω_r and ζ_r of two modes. Finally the matrix $\mathbf{C}_d$ of material damping is found.

5. Numerical results

The material properties and geometric dimensions of the piezoceramic bimorph and nickel beam [12] are listed in Table 1. In the numerical simulations, the voltage $V_{cc} = 100\,\mathrm{V}$ is applied from the initial time and the error tolerance 10^{-9} of Runge–Kutta integration is taken. The initial conditions $\mathbf{Q}$ and $\dot{\mathbf{Q}}$ at $t = 0$ are zero for the forced vibrations, which are caused by the applied voltage but not the initially normal force.

5.1. Determination of material stiffness

By using the characteristic Eq. (37), the first three eigenvalues shown as functions of the tip mass and the material stiffness are exhibited in Fig. 2. In Fig. 2(a), as the material stiffness increases, the first eigenvalue increases from 2.7866 to 3.2483 (A to B), the second eigenvalue increases from 3.6122 to 6.5562 (C to D) and the third eigenvalue increases from 7.0208 to 10.0048 (E to F). In Fig. 2(b), as the tip mass increases, the first eigenvalue decreases from 2.9235 to 1.3556 (B to A), the second eigenvalue decreases from 4.0253 to 3.2536 (D to C) and the third eigenvalue decreases from 7.6706 to 6.5792 (F to E). It is obvious from Figs. 2(a, b) that the eigenvalues

Table 1
Material properties and geometric dimensions of the piezoelectric cantilever bimorph beam designed for the measuring device

	Nickel	Piezoceramic
Young's modulus E (N/m^2):	$E_b = 1.221 \times 10^{10}$	$E_p = 6.3 \times 10^{10}$
Density ρ (kg/m^3):	$\rho_b = 7500$	$\rho_p = 7600$
h_{31} (N/C):		7.182×10^8
β_{33} (V m/C):		6.369×10^6
Length ℓ (mm):	$\ell_b = 69.94$	$\ell_p = 8.00$
Width w (mm):	$w_b = 3.45$	$w_p = 3.45$
Thickness t (mm):	$t_b = 0.50$	$t_p = 0.50$

increase as the material stiffness increases and the tip mass decreases. The material stiffness K could be calibrated from Fig. 2(a), once the natural frequency ω is actually measured by, for example, an optical microscope, and then to calculate the eigenvalue $\beta_2 = \pi\sqrt{\omega}$.

For the special case, $K \to \infty$, the first three eigenvalues are $\beta_2^{(1)} = 3.2483$, $\beta_2^{(2)} = 6.5562$ and $\beta_2^{(3)} = 10.0048$ which are the same as those of the clamped–clamped beam [10]. The first three eigenvalues are $\beta_2^{(1)} = 1.3556, \beta_2^{(2)} = 3.2536$ and $\beta_2^{(3)} = 6.5792$ for the case $M \to \infty$.

Since the eigenvalues are distinct for the given M and K, the sensitivity analyses are also distinct. By using Figs. 2(a) and 2(b), we obtain the derivative of β_2 with respect to K and the derivative of β_2 with respect to M, respectively. Thus, the first-order sensitivity analysis of the eigenvalues can be obtained and the numerical results of the sensitivity analysis are shown in Fig. 3. It is seen from Fig. 3(a) that the sensitivity of the first eigenvalue with respect to the material stiffness has the maximum value at start point A and it has the largest change than the other higher eigenvalues. Thus, the measuring in the material stiffness is preferable by using the first-mode frequency. From Fig. 3(b), it is seen that the sensitivity of the first eigenvalue with respect to the tip mass has the smallest change than the other higher eigenvalues.

In the simple case that the two piezoelectric layers are neglected and $L \approx 0$, by using the characteristic equation (39), the first and second resonant frequencies are shown as functions of the material stiffness and the tip mass in Figs. 4 and 5, respectively. The phenomenon is observed in Fig. 4 that as the material stiffness increases the frequencies increase, and in Fig. 5 that as the tip mass increases the frequencies decrease. Considering the special case, $M = K = 0$, the first and second eigenvalues are $\beta^{(1)} = 1.8751$ and $\beta^{(2)} = 4.6941$, which are the same as those of the clamped–free beam [10], and can be obtained by reducing Eq. (39) as $1 + \cos\beta\cosh\beta = 0$.

In Fig. 4, it can be seen that the values of M and β have the same order in magnitude, but the value of K may approach infinity. As the special case $K \to \infty$, Eq. (39) can be reduced to as $\sin\beta\cosh\beta - \sinh\beta\cos\beta = 0$, which can be solved for $\beta^{(1)} = 3.9266$ and $\beta^{(2)} = 7.0686$ as shown in Figs. 4(a) and (b), respectively. This is the limit case for $k \gg E_b I_b/\ell_b^3$, i.e., the stiffness to be measured is much larger than that of the cantilever beam. In Fig. 5, the parameter M of the tip mass is chosen from 0 to 0.20 for practical applications [13,14]. In these ranges, the curves shown in Figs. 5(a) and (b) are almost linear for the first and second eigenvalues.

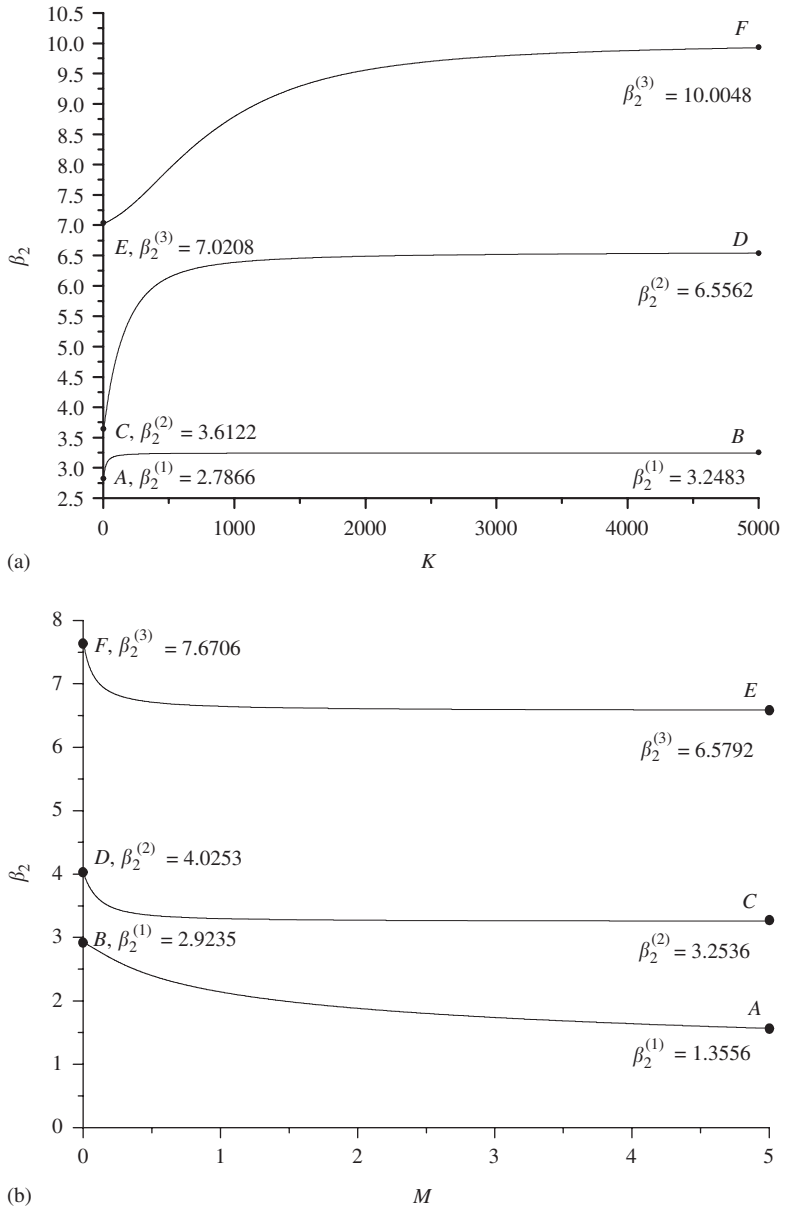

Fig. 2. The first three eigenvalues are shown as functions of the material stiffness and tip mass. (a) The eigenvalues versus the material stiffness in case of $M = 0.1104$. (b) The eigenvalue versus the tip mass in case of $K = 0$.

The numerical results of sensitivity analysis with respect to the material stiffness (40) and the tip mass (41) are shown in Figs. 6(a) and (b), respectively. In Fig. 6(a), the sensitivity $d\beta/dK$ for the special case $M = 0$ has the maximum at points A and C, and has zeros at points B and D for the first and second eigenvalues, respectively. In Fig. 6(b), the sensitivity $d\beta/dM$ for the special case

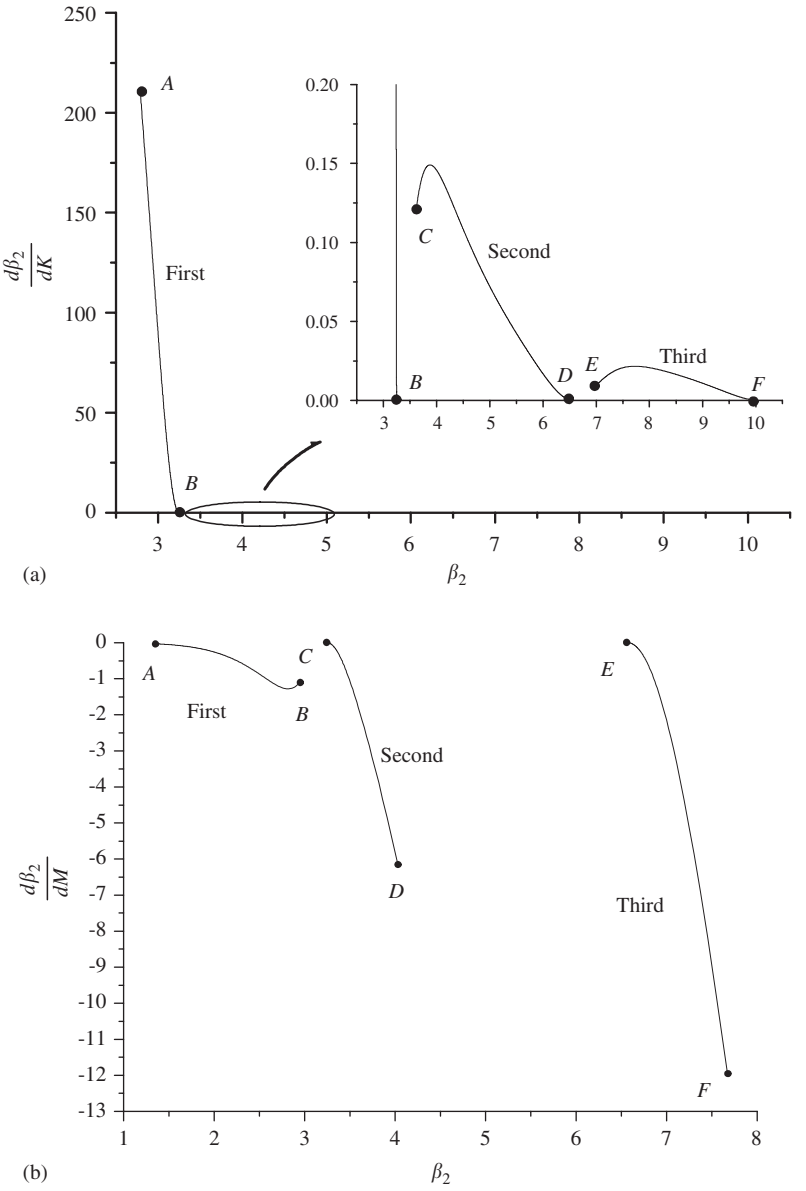

Fig. 3. The sensitivity analyses of the eigenvalues. (a) The sensitivity with respect to the material stiffness with $M = 0.1104$. (b) The sensitivity with respect to the tip mass without the material stiffness.

$K = 0$ has the zeros at points A and C, and has minimum at points B and D for the first and second eigenvalues, respectively.

Numerical simulations by the finite element method are presented for the transverse vibrations, in which five elements with convergent error 10^{-9} of Runge–Kutta integration are taken and the constant voltage $V_{cc} = 100\,\mathrm{V}$ is applied. The transverse vibrations shown in Fig. 7(a) with

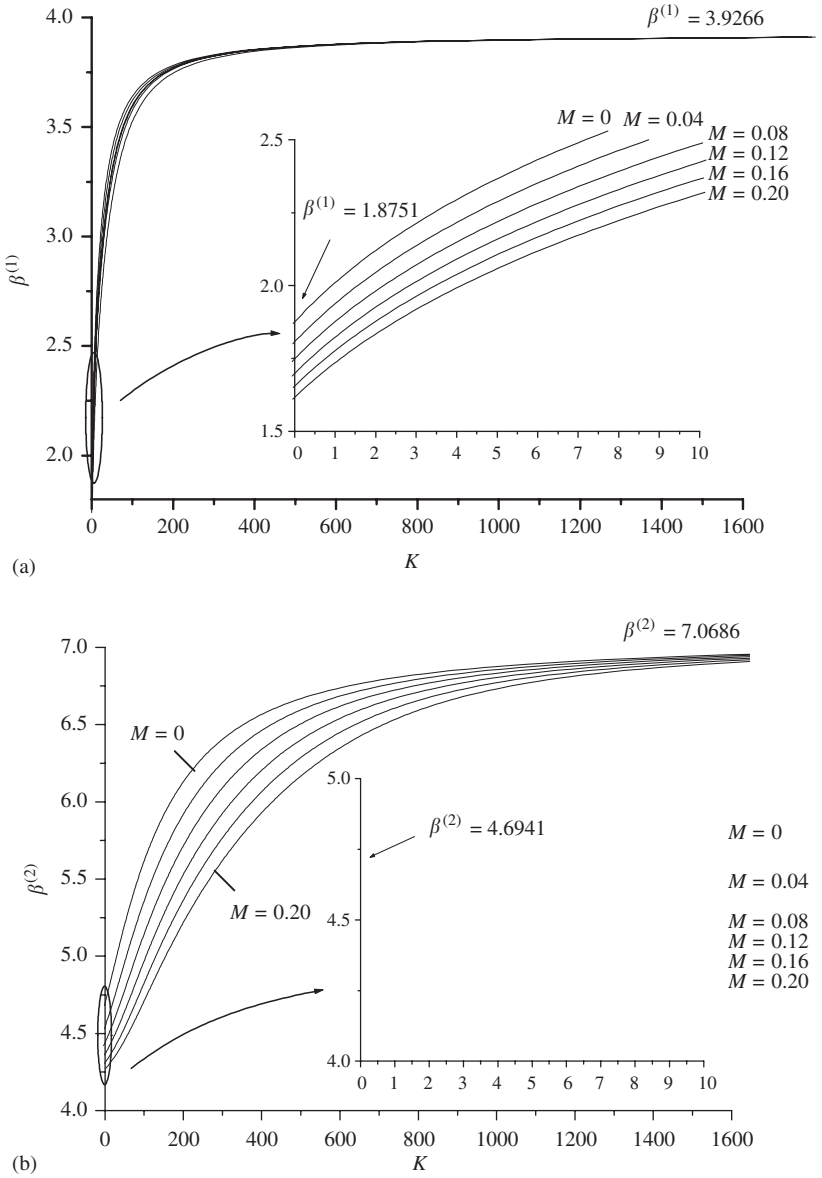

Fig. 4. The eigenvalues as functions of material stiffness could be determined for various values of tip masses $M = 0-0.20$. (a) The first eigenvalue. (b) The second eigenvalue.

$k = 171.6\,\mathrm{N/m}$, $m = 0.0001\,\mathrm{kg}$ and $f = 0\,\mathrm{N}$ for different damping can be transformed to their frequency spectrum by using the fast Fourier transform (FFT) as shown in Fig. 7(b) for the first three modes. From Fig. 7(b), we can obtain $\omega_1 = 110\,\mathrm{Hz}$. With the dimensionless frequency $\omega = 2\pi\omega_1\sqrt{\rho_b A_b \ell_b^4/\pi^4 E_b I_b} = 0.99$ and the eigenvalue $\beta_2 = \pi\sqrt{\omega} = 3.12$, we calibrate the

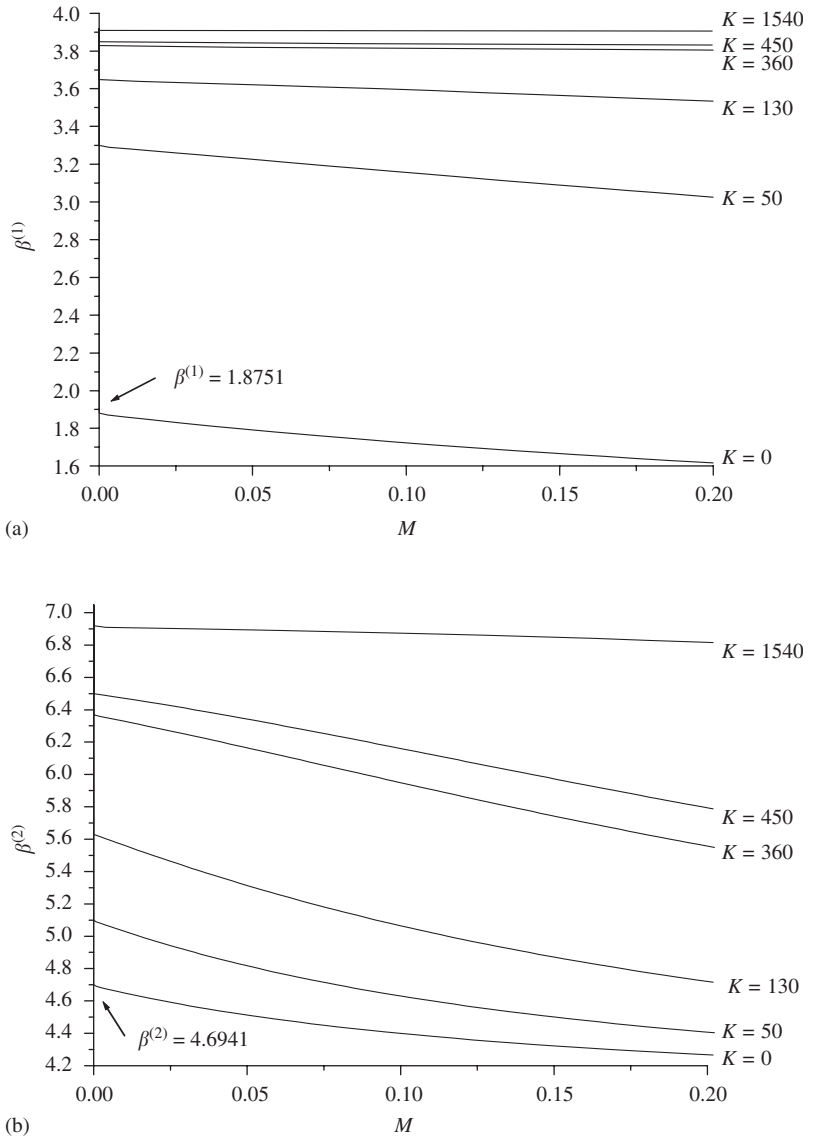

Fig. 5. The eigenvalues as functions of tip mass could be determined for various values of material stiffnesses $K = 0-1540$. (a) The first eigenvalue. (b) The second eigenvalue.

dimensionless material stiffness $K = 33$ from Fig. 2(a), and calculate the measured material stiffness 168.8 N/m. It is found that the error is 1.63%.

5.2. Determination of material damping

The transverse vibrations and their frequency spectrum are shown in Figs. 7(a) and (b), respectively. It is found that the amplitudes and the spectrum decrease by increasing the damping.

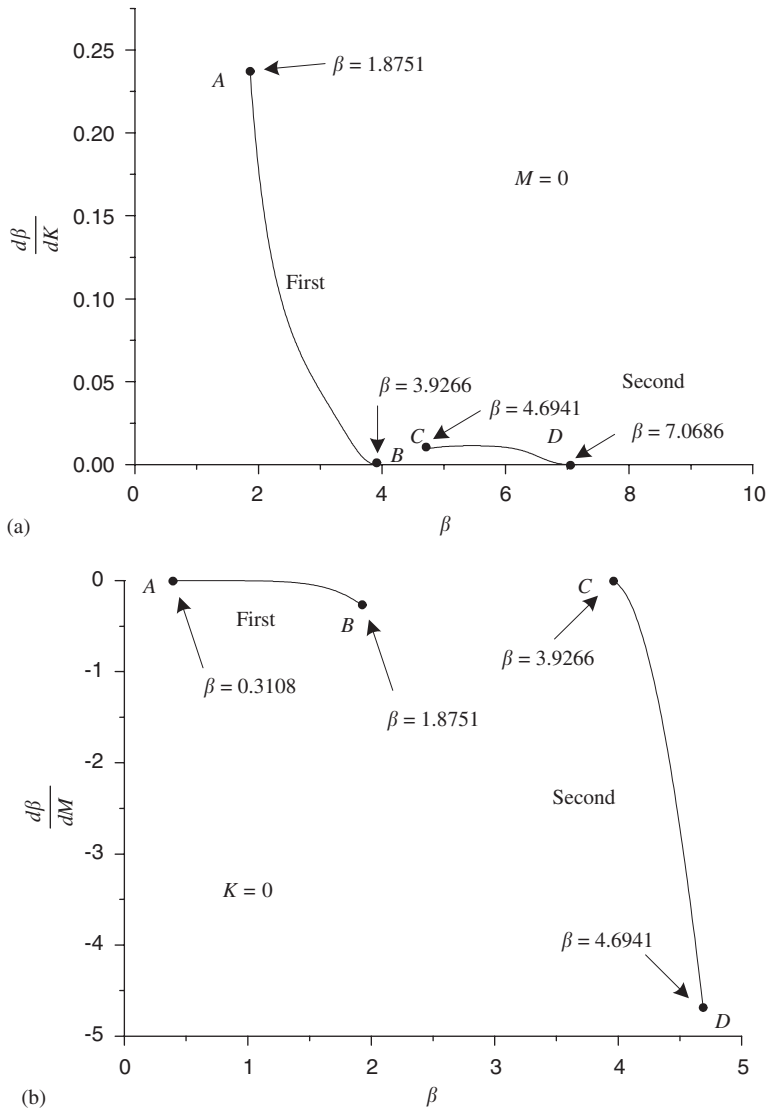

Fig. 6. The sensitivity analyses of eigenvalues. (a) Without the tip mass, the sensitivity of eigenvalue with respect to the material stiffness. (b) Without the material stiffness, the sensitivity of eigenvalue with respect to the tip mass.

Since there are two constants $\bar{\alpha}$ and $\bar{\beta}$ in Eq. (56) to be determined, it at least needs two modes of $\omega_r^{(1)}, \omega_r^{(2)}$ and ω_r from Fig. 8 to obtain ζ_1 and ζ_2 by using Eq. (46). From the practical calculation, we obtain from Eq. (56) the two constants $\bar{\alpha} = 10.06$ and $\bar{\beta} = 4.7\text{E} - 6$, and by using Eq. (54) we obtain the damping matrix as

$$\mathbf{C}_d = 10.06\mathbf{M}_d + 4.7\text{E} - 6\mathbf{K}_d. \tag{57}$$

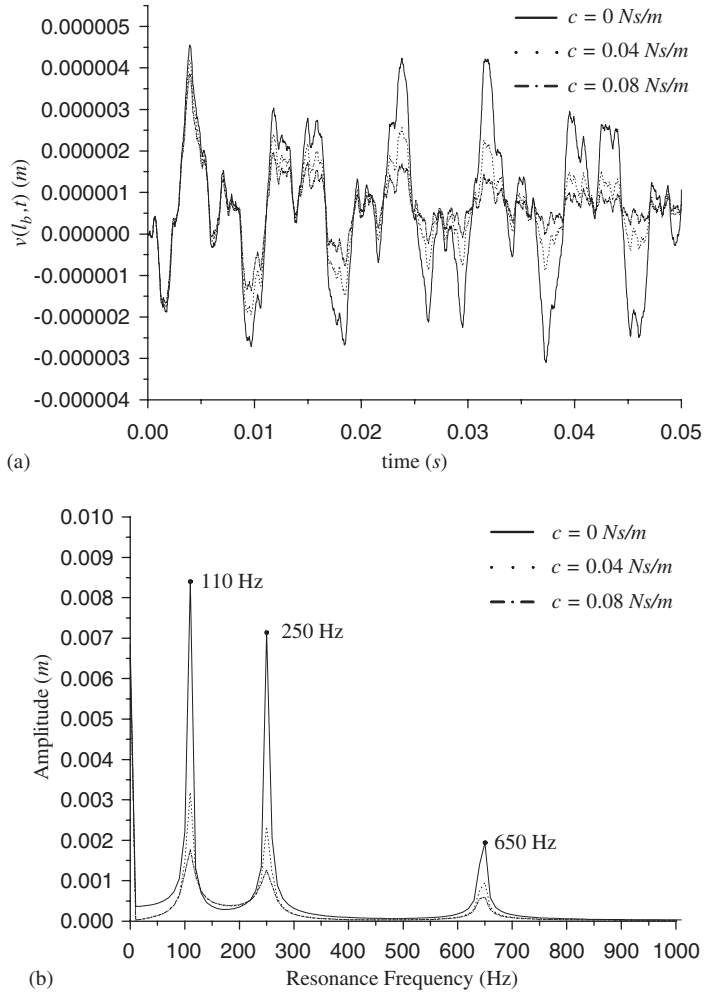

Fig. 7. (a) The transverse vibrations and (b) the spectrum with $k = 171.6\,\mathrm{N/m}$, $m = 0.0001\,\mathrm{kg}$ and $f = 0\,\mathrm{N}$ for different dampers: $c = 0\,\mathrm{Ns/m}-$, $c = 0.04\,\mathrm{Ns/m}\cdots$ and $c = 0.08\,\mathrm{Ns/m}\ -\cdot-$, and a constant voltage $V_{cc} = 100\,\mathrm{V}$.

Consequentially, the measured damping coefficient is 0.0404 Ns/m, and the error is about 2.0%. The other different damper coefficients can be obtained in the same way and shown in Table 2, where all the errors are less than 3.5%.

6. Conclusions

The triple-layer piezoelectric cantilever bimorph beam is successfully formulated based on the general concept of the constitutive laws of piezoelectric materials and the introduction of kinetic and strain energies in Hamilton's principle. In this paper, the method to measure material

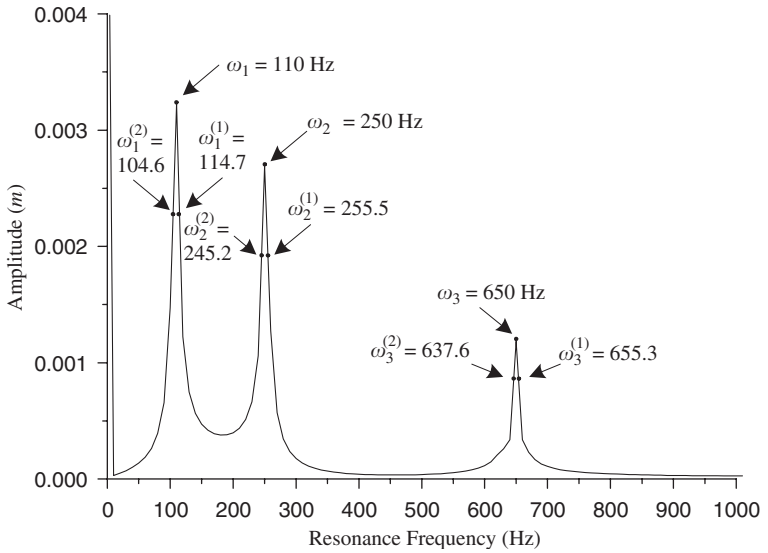

Fig. 8. The spectrum with $k = 171.6\,\mathrm{N/m}$, $m = 0.0001\,\mathrm{kg}$ and $f = 0\,\mathrm{N}$ for the damper: $c = 0.04\,\mathrm{Ns/m}$, and a constant voltage $V_{cc} = 100\,\mathrm{V}$.

Table 2
Material damping coefficients c, damping ratios ζ_1 and ζ_2, proportionality constants $\bar{\alpha}$ and $\bar{\beta}$, the calculated damping coefficients c' and the errors

c (Ns/m)	ζ_1	ζ_2	$\bar{\alpha}$	$\bar{\beta}$	c' (Ns/m)	Error (%)
0.01	0.0345	0.0164	7.46	1.01E − 6	0.0101	1.0
0.02	0.0458	0.0206	10.05	2.21E − 6	0.0204	2.0
0.04	0.0459	0.0207	10.06	4.72E − 6	0.0406	2.0
0.06	0.0464	0.0228	10.90	7.40E − 6	0.0619	3.2
0.08	0.0687	0.0312	14.99	9.80E − 6	0.0827	3.4

viscoelasticity is proposed. The analytical model could predict the material stiffness from the measurement of the resonant frequencies, and the damping coefficient from the spectrum. The examples, showing the procedures of determining these coefficients, are provided. From the sensitivity analyses, the measuring in material stiffness is preferable by using the first-mode frequency.

Acknowledgment

Support of this work by the National Science Council of the Republic of China Contract NSC-91-2212-E-327-006 is gratefully acknowledged. The first author wishes to thank Prof. Jyh-Horng Chou for his discussion on the damping.

Appendix A

The coefficients of the shape function (36) of the piezoelectric cantilever bimorph beam are

$$
\begin{aligned}
A_1 &= -C_1 \\
&= A_2\left\{\frac{\sin\beta_2\mu^+(\cos\beta_1\mu^- - \cosh\beta_1\mu^-)(\sin\beta_1\mu^- + \sinh\beta_1\mu^-)}{(2-2\cos\beta_1\mu^-\cosh\beta_1\mu^-)(\cos\beta_1\mu^- - \cosh\beta_1\mu^-)}\right. \\
&\quad \left. + \frac{-\frac{\beta_2}{\beta_1}\cos\beta_2\mu^+(\sin^2\beta_1\mu^- - \sinh^2\beta_1\mu^- - (2-2\cos\beta_1\mu^-\cosh\beta_1\mu^-))}{(2-2\cos\beta_1\mu^-\cosh\beta_1\mu^-)(\cos\beta_1\mu^- - \cosh\beta_1\mu^-)}\right\} \\
&\quad + B_2\left\{\frac{\cos\beta_2\mu^+(\cos\beta_1\mu^- - \cosh\beta_1\mu^-)(\sin\beta_1\mu^- + \sinh\beta_1\mu^-)}{(2-2\cos\beta_1\mu^-\cosh\beta_1\mu^-)(\cos\beta_1\mu^- - \cosh\beta_1\mu^-)}\right. \\
&\quad \left. + \frac{\frac{\beta_2}{\beta_1}\sin\beta_2\mu^+(\sin^2\beta_1\mu^- - \sinh^2\beta_1\mu^- - (2-2\cos\beta_1\mu^-\cosh\beta_1\mu^-))}{(2-2\cos\beta_1\mu^-\cosh\beta_1\mu^-)(\cos\beta_1\mu^- - \cosh\beta_1\mu^-)}\right\} \\
&\quad + C_2\left\{\frac{\sinh\beta_2\mu^+(\cos\beta_1\mu^- - \cosh\beta_1\mu^-)(\sin\beta_1\mu^- + \sinh\beta_1\mu^-)}{(2-2\cos\beta_1\mu^-\cosh\beta_1\mu^-)(\cos\beta_1\mu^- - \cosh\beta_1\mu^-)}\right. \\
&\quad \left. + \frac{-\frac{\beta_2}{\beta_1}\cosh\beta_2\mu^+(\sin^2\beta_1\mu^- - \sinh^2\beta_1\mu^- - (2-2\cos\beta_1\mu^-\cosh\beta_1\mu^-))}{(2-2\cos\beta_1\mu^-\cosh\beta_1\mu^-)(\cos\beta_1\mu^- - \cosh\beta_1\mu^-)}\right\} \\
&\quad + D_2\left\{\frac{\cosh\beta_2\mu^+(\cos\beta_1\mu^- - \cosh\beta_1\mu^-)(\sin\beta_1\mu^- + \sinh\beta_1\mu^-)}{(2-2\cos\beta_1\mu^-\cosh\beta_1\mu^-)(\cos\beta_1\mu^- - \cosh\beta_1\mu^-)}\right. \\
&\quad \left. + \frac{-\frac{\beta_2}{\beta_1}\sinh\beta_2\mu^+(\sin^2\beta_1\mu^- - \sinh^2\beta_1\mu^- - (2-2\cos\beta_1\mu^-\cosh\beta_1\mu^-))}{(2-2\cos\beta_1\mu^-\cosh\beta_1\mu^-)(\cos\beta_1\mu^- - \cosh\beta_1\mu^-)}\right\}, \qquad \text{(A.1)}
\end{aligned}
$$

$$
\begin{aligned}
B_1 &= -D_1 \\
&= A_2\left[\frac{\sin\beta_2\mu^+(\cos\beta_1\mu^- - \cosh\beta_1\mu^-) - \dfrac{\beta_2}{\beta_1}\cos\beta_2\mu^+(\sin\beta_1\mu^- - \sinh\beta_1\mu^-)}{(2-2\cos\beta_1\mu^-\cosh\beta_1\mu^-)}\right] \\
&\quad + B_2\left[\frac{\cos\beta_2\mu^+(\cos\beta_1\mu^- - \cosh\beta_1\mu^-) + \dfrac{\beta_2}{\beta_1}\sin\beta_2\mu^+(\sin\beta_1\mu^- - \sinh\beta_1\mu^-)}{(2-2\cos\beta_1\mu^-\cosh\beta_1\mu^-)}\right] \\
&\quad + C_2\left[\frac{\sinh\beta_2\mu^+(\cos\beta_1\mu^- - \cosh\beta_1\mu^-) - \dfrac{\beta_2}{\beta_1}\cosh\beta_2\mu^+(\sin\beta_1\mu^- - \sinh\beta_1\mu^-)}{(2-2\cos\beta_1\mu^-\cosh\beta_1\mu^-)}\right] \\
&\quad + D_2\left[\frac{\cosh\beta_2\mu^+(\cos\beta_1\mu^- - \cosh\beta_1\mu^-) - \dfrac{\beta_2}{\beta_1}\sinh\beta_2\mu^+(\sin\beta_1\mu^- - \sinh\beta_1\mu^-)}{(2-2\cos\beta_1\mu^-\cosh\beta_1\mu^-)}\right]. \qquad \text{(A.2)}
\end{aligned}
$$

References

[1] G. Binning, C.F. Quate, C. Gerber, Atomic force microscope, *Physical Review Letters* 56 (1986) 930–933.

[2] R.F. Fung, S.C. Huang, Dynamic modeling and vibration analysis of the atomic force microscope, *Journal of Vibration and Acoustics* 123 (2001) 502–509.

[3] E. Finot, T. Thundat, E. Lesniewska, J.P. Goudonnet, Measuring magnetic susceptibilities of nanogram quantities of materials using microcantilevers, *Ultramicroscopy* 86 (2001) 175–180.

[4] T.L. Porter, M.P. Eastman, D.L. Pace, M. Bradley, Sensor based on piezoresistive microcantilever technology, *Sensors and Actuators A* 88 (2001) 47–51.

[5] H.F. Ji, K.M. Hansen, Z. Hu, T. Thundat, Detection of pH variation using modified microcantilever sensors, *Sensors and Actuators B* 72 (2001) 233–238.

[6] L. Wang, The role of damping in phase imaging in tapping mode atomic force microscopy, *Surface Science* 429 (1999) 178–185.

[7] E. Kester, U. Rabe, L. Presmanes, P. Tailhades, W. Arnold, Measurement of Young's modulus of nanocrystalline ferrites with spinel structures by atomic force acoustic microscopy, *Journal of Physics and Chemistry of Solids* 61 (2000) 1275–1284.

[8] N. Guo, P. Gawley, D. Hitchings, The finite element analysis of the vibration characteristics of piezoelectric discs, *Journal of Sound and Vibration* 159 (1992) 115–138.

[9] R.F. Fung, C.M. Yao, C.R. Tseng, Dynamic analysis of a bimodal ultrasonic motor with initially stressed force onto the rotor, *Sensors and Actuators A* 72 (1999) 115–138.

[10] L. Meirovitch, *Fundamentals of Vibrations*, McGraw-Hill International Editions, Singapore, 2001.

[11] S.H. Chang, Quantitative Determination of Material Viscoelasticity using a Piezoelectric Cantilever Bimorph Beam, Master's Thesis, Kaohsiung First University of Science and Technology, Kaohsiung, Yenchau, Taiwan, 2002.

[12] M.F. Coughlin, D. Stamenovic, J.G. Smits, Determining spring stiffness by the resonance frequency of cantilevered piezoelectric bimorphs, *IEEE Transactions on Ultrasonics, Ferroelectrics, and Frequency Control* 44 (4) (1997) 730–732.

[13] S. Amelio, A.V. Goldade, U. Rabe, V. Scherer, B. Bhushan, W. Arnold, Measurements of elastic properties of ultra-thin diamond-like carbon coatings using atomic force acoustic microscopy, *Thin Solid Films* 392 (2001) 75–84.
[14] U. Rabe, K. Janser, W. Arnold, Vibrations of free and surface-coupled atomic force microscope cantilevers: theory and experiment, *Review of Scientific Instruments* 67 (9) (1996) 3281–3293.
[15] A.D. Nashif, D.I.G. Jones, J.P. Henderson, *Vibration Damping*, Wiley, New York, 1984 (Chapter 4).
[16] C.W. Bert, Material damping: an introductory review of mathematical models, measures and experimental techniques, *Journal of Sound and Vibration* 29 (1973) 129–153.
[17] J.N. Reddy, *An Introduction to the Finite Element Method*, second ed., McGraw-Hill International Editions, Singapore, 1993 (Chapter 14).
[18] V. Balamurugan, S. Narayanan, Finite element formulation and active vibration control study on beams using smart constrained layer damping (SCLD) treatment, *Journal of Sound and Vibration* 249 (2) (2002) 227–250.